Journal of Non-Crystalline Solids 356 (2010) 1620–1625

Contents lists available at ScienceDirect

Journal of Non-Crystalline Solids

journal homepage: www.elsevier.com/ locate/ jnoncrysol

Hexamethylenetetramine multiple catalysis as a porosity and pore size modifier in carbon cryogels

Betzaida Batalla García, Dawei Liu, Saghar Sepehri, Stephanie Candelaria, David M. Beckham, Leland W. Savage, Guozhong Cao *

University of Washington, Materials Science and Engineering, 302 Roberts Hall, Seattle, WA 98195-2120, United States

ARTICLE INFO

Article history:
Received 22 October 2009
Available online 23 July 2010

Keywords:
Sol–gel;
Catalysis;
Porous material;
Polymer

ABSTRACT

Hexamethylenetetramine (HMTA) base catalysis is used to control the porosity and pore size of resorcinol furaldehyde cryogels synthesized in tert-butanol. While HMTA produces ammonia and formaldehyde in aqueous media, other carbon–nitrogen molecular units are possible in non-aqueous solvents. The results suggest that at least two paths are possible from this decomposition, a reactive catalyst in pure tert-butanol or a base like catalyst in an aqueous mix. Due to the catalytic effect under high catalysis in tert-butanol the samples promoted high macroporosity >70%, reduced shrinkage <20% and had lower syneresis compared to specimens with low concentration of HMTA. On the other hand the use of water mixtures was shown to reduce the mesopore size up to 50%, and reduce the macroporosity to 20%, when compared to the tert-butanol case. Nitrogen physisorption, TEM and FTIR are used to characterize the chemical and structural properties of the cryogels.

© 2010 Elsevier B.V. All rights reserved.

1. Introduction

Hexamethylenetetramine (HMTA or hexamine), $C_6H_{12}N_4$, amine base catalyst can be particularly beneficial to the synthesis of phenolic gels used as precursors for mesoporous carbons especially those found in electrodes for electrical energy storage applications [1–3]. The gels have tunable nanoporous structure an important parameter in the performance of supercapacitors [2], there is no metal ion impurities and the polymerization reactions take place in an organic solvent directly thus, the wet gels are ready for solvent removal by either supercritical, ambient or freeze drying [4,5]. This aspect of HMTA present an advantage over most traditional metal base catalyzed gels prepared in aqueous solutions, which require a solvent exchange and other treatments to retain their nanoporous structure during the drying process [6]. Unfortunately, unlike metal ion catalysis, the polycondensation reaction catalyzed by hexamine so far limited the tunability of the mesopore size to a diameter >20 nm [4,5] and further below 20 nm has proven difficult. A limit imposed by the base reaction is usually responsible for the pore size reduction. In metal hydroxide catalysis, pH and the metal ion size determine the rate of reaction that controls the pore size [7,8]. But, HMTA has additional chemical properties since it is a Lewis base and its electron donation or basicity highly depends on the pH of the solvent. The pH also can promote HMTA to decompose and add functional groups to the polymer network as a catalytic reactant and alter the overall nanostructure. Therefore, if the organic solvent pH is taken into account this amine base can further transform the sol–gel structure in more than one way or even remove the mesopore size limitations among other aspects.

For example, mixtures of tert-butanol (t-BuOH) and water have been studied [9–11] and have shown that the water alcohol mixture affect the H^+ concentration. The donation of protons from water to the alcohol and the increase in OH^- in the mixture are important when using amine bases because of their nucleophilic nature. Amine nucleophilicity can be seen as electron donors or proton acceptors for which the concentration of H^+ can affect the amine bases catalytic effect. Also, the presence of other nucleophilic or electrophilic species like aldehydes can further alter the reaction. An example is bifunctional catalysis of amines producing imino anions and enolates, in the case of hexamine also decomposition into formaldehyde and ammonia when reacted with water ($C_6H_{12}N_4 + 6H_2O \rightleftharpoons 6CH_2O + 4NH_3$) [12–14]. Denmak et al. have recently published an extensive review on Lewis bases including this subject in more detail [15].

Similar behavior of HMTA was observed by Wu et al. who used hexamine as a base catalyst to produce resorcinol furaldehyde aerogels in organic solvents [5]. The gels reported have nanoporous structure but when the HMTA catalyst is used in high concentration ($R/C \leq 50$) it also takes place in the polymerization, which is attributed to the decomposition of HMTA into formaldehyde and ammonia. However studies in phenolic polycondensation have shown also that it is possible to decompose into imines, amides etc… (nitrogen analogs of aldehydes [16]) during the preparation of phenolic resins.

* Corresponding author.
E-mail address: gzcao@u.washington.edu (G.Z. Cao).

0022-3093/$ – see front matter © 2010 Elsevier B.V. All rights reserved.
doi:10.1016/j.jnoncrysol.2010.06.033

The polymerization mechanisms in such phenolic resins are discussed in detail by Zhang [17,18]. It is suggested that the formation of imine, amide and imide bridges are possible by the removal of water from the solvent during the synthesis. Therefore the decomposition path from imine to aldehyde can be controlled through altering the sol–gel reactions by varying the content of water and or pH value. The resulting sol–gel polycondensation using hexamine is that of a non stoichiometric condition in which an aldehyde-ammonia system or a catalytic reactant (like imines etc…) are possible. These reactions in turn can alter the pore structure.

In this publication a group of phenolic gels is prepared using resorcinol and furaldehyde in an organic solvent (tert-butyl alcohol), to determine the roles of hexamine in the gelation process and the structural properties of the gel. The solid content, hexamine concentration and solvent chemistry (tert-butyl alcohol/water mixtures) are evaluated for chemical and structural properties. The results are also compared to those of ion catalyzed gels of similar structure.

2. Experimental

Samples were prepared using the monomers resorcinol, furaldehyde and HMTA (resorcinol, furaldehyde and HMTA, were purchased from Sigma Aldrich). Although similar synthesis has been developed by Wu et al. [5], the new synthesis also used the solvent's chemistry and pH. I.e. the polycondensation reaction took place in solvent mixtures of tert-butanol and water. The furaldehyde to resorcinol (FR) molar ratio was set to 2.5 and the resorcinol to HMTA (RH) molar ratios were between 25 and 100. The reactants were added first, the monomers (resorcinol and furaldehyde), the solvent and last the catalyst. To completely dissolve the catalyst the samples were heated to 80 °C for 60 min then mixed for 15 min in an ultrasonic bath and placed in the oven at the same temperature. The solvent chosen was tert-butyl alcohol (from here on referred as t-BuOH) commonly used in freeze drying. The solvent mixture with t-BuOH had DI water concentrations (X_{H_2O}) between 3 and 11 mM (corresponding to 5 to 20% volume of water). Two solid contents 35% and 45% were used. The solid content is calculated using the weight percent ratio of monomers to the solution in t-BuOH. Sample preparation is summarized in Tables 1 and 2. Samples were freeze dried under vacuum at −50 °C in a Labconco FreeZone 1 L Freeze dryer. Pyrolysis was performed under N_2 at a ramp rate of 5 °C/min at a maximum temperature of 900 °C for 180 min.

2.1. FTIR and CHN analysis

Fourier transform infrared (FTIR) was performed using a Thermo Scientific Nicolet 6700 FTIR Spectrometer with a deuterated triglycine sulfate detector (DTGS) to use with potassium bromide (KBr). Samples were mixed in a 1:200 ratio of polymer to KBr and measured in dry air. The sampling, resolution and range were 256 scans, 4 cm^{-1} and 4000 to 400 cm^{-1}. CHN (carbon, hydrogen and nitrogen) analysis was used to support the FTIR scans using a Pekin Elmer Co. CHN 2400 Analyzer was at a combustion temperature of 950 °C.

Table 1
Sample preparation for t-BuOH alcohol and water t-BuOH mixture samples and metal ion base samples, resorcinol formaldehyde (RF) and resorcinol furaldehyde (RFF).

ID	RC	Solvent	% Solids	ID	RC	Solvent	% Solids
$A_{45}c$	50	t-BuOH	45	RF	50	Water	ca. 25
$A_{35}a$	100	t-BuOH	35	RFF	50	t-BuOH	45
$A_{35}c$	50	t-BuOH	35	$H_{35}a$	100	t-BuOH + H_2O[a]	35
$A_{35}d$	25	t-BuOH	35	$H_{35}d$	25	t-BuOH + H_2O[a]	35

[a] The concentration of water in t-BuOH + H_2O is 8 mM.

Table 2
Sample preparation for BET and structural tests.

DI Water				Hexamine			
ID	RH	X_{H_2O} (mM)	% Solids	ID	RH	X_{H_2O} (mM)	% Solids
$W_{35}a$	50	3	35	$H_{35}a$	100	8	35
$W_{35}b$	50	5	35	$H_{35}b$	75	8	35
$W_{35}c$	50	8	35	$H_{35}c$	50	8	35
$W_{35}d$	50	11	35	$H_{35}d$	25	8	35
$W_{45}c$	50	8	45	–	–	–	–

The concentration increases from a to d for X_{H_2O} and RH.

2.2. Structural measurements, N_2 physisorption, bulk density and TEM

The nitrogen sorption was done using a NOVA 4200e. The total surface area (SA) was determined using the multi point BET method. The t-method was used to measure the micropore volume. The micropore size distribution was measured using the DA method. For the mesopore volume the BJH method was used. The desorption isotherm was used to generate the pore size distributions [19]. Bulk density measurements were performed using a modified version of ASTM C20-00, in isobutanol to determine the macropore volume using the external volume of the samples and graphite's density to calculate the solid volume. Transmission electron microscopy measurements were done using a (JSM 2010, Philips JEOL).

3. Results and discussion

3.1. The sol–gel process

The sol–gel process is the first stage in which the impact of HMTA's catalysis in the various scenarios can be observed. Immediately after mixing the precursor solutions the color was a dark brown for all samples. The various combinations are listed in Tables 1 and 2. The samples with t-BuOH had to be heated (80 °C) to mix the hexamine completely while in the mixtures of water and t-BuOH the hexamine dissolved readily (see Experimental section). After 24 h all the samples had gone trough gelation with differences in color and transparency. However under high catalyst concentration, RH = 25, the addition of water decreased the gelation time by 2.5 h compared to t-BuOH alone (3 vs. 5.5 h in t-BuOH). This time reduction can be attributed to the increase in basicity from the ammonia when the water decomposes the hexamine.

The color of the samples in t-BuOH, $A_{35}a$ to d, with low catalyst concentration (RH = 100) was dark brown similar to the RF gels. Those with high catalyst ranged from gray, $A_{35}c$ (RH = 50) to yellow-orange, $A_{35}d$ (RH = 25). The yellow-orange (λ ca. 600 nm) coloration is also ascribed to imine polymers [20]. However, adding water under similar catalytic conditions the color was brown for all as seen in Fig. 1.

After aging for seven days, the syneresis of the gels varied with the amount of catalyst and solvent type. In t-BuOH, low catalyst concentration had the most syneresis while the samples with high catalyst concentration had no detectable syneresis. The samples that used the solvent mixture were more prone to syneresis as the water amount was increased. Removal of the solvent using freeze drying produced other physical changes. The samples in the t-BuOH alcohol had the lowest amount of shrinkage at high RH concentrations of 25 and 50 ($A_{35}a$ and c) with 13 and 28% in volume reduction respectively. However, those tested under similar conditions using 8 mM of water had increased shrinkage, in the range of 37 to 49% after drying. After pyrolysis the samples experience an additional 20% shrinkage in the t-BuOH case $A_{35}c$ and 50 to 80% in the water case $W_{35}a$ to d.

The sol–gel processing shows differences between the Hexamine system in t-BuOH and when water is introduced. The changes in color, syneresis and shrinkage after drying relate to chemical and structural

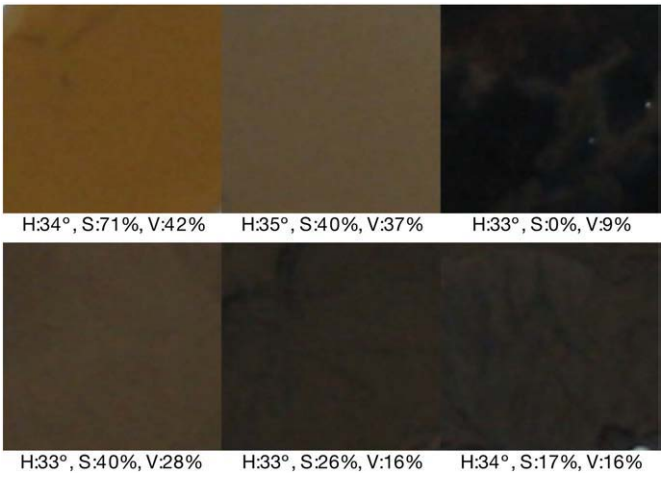

Fig. 1. Top row are samples prepared using various catalyst amounts in t-BuOH. The color changes (from left to right) from yellow-orange (RH = 25) to gray (RH = 50) to dark brown (RH = 75). Bottom, their counterparts prepared with 8 mM water mixtures have same catalyst amount but are all brown. Average hue, H, saturation, S, and value, V, and numbers of the selected portions are provided to simplify the comparison when a color display is not available.

alterations from two catalytic mechanisms. Notice in the case of HMTA in t-BuOH the low syneresis and shrinkage with the increase concentration of catalyst is uncommon of gels with high catalytic effect in metal base catalysis [7,21]. This implies that HMTA acts as more than just a catalyst. However, the shrinkage increases with the addition of water in a similar fashion to the metal ion counterparts. Notice also that the gelation time does not differ greatly between the t-BuOH and water systems leaving the differences not to the reaction rate but to a different chemical species. The structural changes produced by HMTA can be seen in more detail in the nitrogen physisorption measurements.

3.2. Pore structure

3.2.1. Effect of solid content

The solid content was found to significantly reduce the pore size distribution. Under the same catalytic conditions, RH = 50, the increase of solid content (35 to 45%) reduced the pore size distribution in the mesopore region. In the t-BuOH alcohol samples, $A_{35}c$ and $A_{45}c$, the mesopore size was broad and large, >30 nm, Fig. 2A, while the micropore size and surface area were preserved, Table 3. Also, the pore volume in the macropore region changed drastically between the two solid contents. At a solid content of 45% the macropore volume was near zero as seen in Fig. 3A.

Compared to the control samples when water is added to the mixture, $W_{35}c$ and $W_{45}c$, the pore size distribution reduces in size by 50% and the overall pore volume is also reduced in Fig. 3C. Notice that combining solid content and H^+ concentration from water a range of pore sizes from 6 to 40 nm can be achieved. See Fig. 2A. This range is not possible using only the organic solvent.

3.2.2. Effect of catalyst, RH

The effect of catalyst is more complex. In the t-BuOH group the mesopore size distribution is present only at an RH = 50 while not present at higher or lower hexamine concentrations. See Table 3, $A_{35}a$ to *d*. But, when water is added a peak forms at 17 nm even at low concentration, RH = 75 and 100, until it vanishes at high concentration, RH = 25. Fig. 2B shows this transition.

As mentioned earlier, a contradictory behavior from metal base catalyzed RF gels is observed in the macropore volume of those samples prepared in t-BuOH, as seen in Fig. 3A, where the macropore volume and porosity increased when increasing the catalyst concentration. That behavior is common of low catalyst concentration in RF gels with low solid content [7,21]. For example, the RF sample produced using a metal ion base in Appendix Table 5 had a macropore volume of 13 cm^3/g (88% porosity). However the micropore volume was nonexistent. But like the metal ion counterparts, in the t-BuOH samples the micropore size is reduced and the micropore volumes are comparable to those seen under high concentration of metal base catalyst in the RFF case, ca. 0.2 cm^3/g (27% porosity) while also keeping high mesopore volumes, as seen in Appendix Table 5.

Under the same circumstance, the addition of 8 mM of water in the solvent produced other changes. The macropore volume decreased at the high catalyst concentration increasing also the mesoporosity, Fig. 3B, $H_{35}a$ to *d*.

It can be seen here that the reduction in shrinkage and syneresis of the gels in the t-BuOH case is due to an increase in the macropore volume which allows easy sublimation or evaporation of the solvent during drying. This macropore volume is reduced by the addition of water increasing the mesopore and micropore porosity and increasing both the shrinkage and syneresis.

3.2.3. Effect of water concentration

The effect of water concentration can be seen in samples $W_{35}a$ to *d*. The water content was increased from 2 to 11 mM while retaining the catalyst and solid content constant, 50 and 35% respectively. The pore size distribution sharpens without changing the mesopore size. A maximum peak is achieved at 8 mM, Fig. 2C. Notice the increase in water content retains the micropore and mesopore volume as seen in Fig. 3C. But a drastic decrease in the macropore volume is observed. This is also consistent with the syneresis and shrinkage observations.

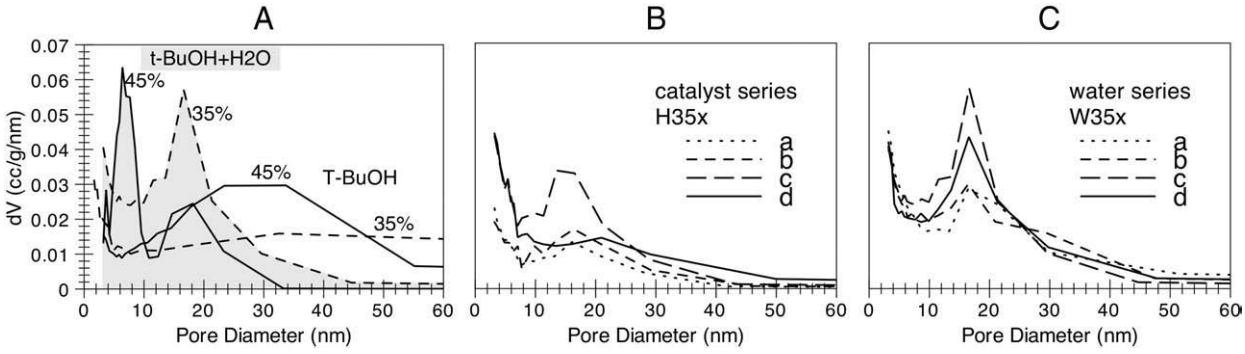

Fig. 2. Pore size distribution of carbon cryogels. The effect of solid content, A, reduces the size of the distribution in both cases control and water. When water is added to the solvent, B, the increase in catalyst reduces the mesopore diameter to ca. 17 nm. Ultimately increasing the water content, C, the distribution becomes narrower while preserving the pore size achieving a maximum at 8 mM.

Table 3
Density, ρ, surface area, S, and pore diameter, D of pyrolyzed samples.

	45% Solids		HMTA + t-BuOH			HMTA + water				Water			
	$A_{45}c$	$W_{45}c$	$A_{35}a$	$A_{35}c$	$A_{35}d$	$H_{35}a$	$H_{35}b$	$H_{35}c$	$H_{35}d$	$W_{35}a$	$W_{35}b$	$W_{35}c$	$W_{35}d$
ρ (g/cm^3)	0.56	0.87	1	0.35	0.28	0.49	0.5	0.38	0.35	0.45	0.49	0.57	0.69
S_{BET} (m^2/g)	575	583	380	593	633	521	470	598	601	575	542	593	532
D_{Micro} (nm)	1.2	1.2	1.58	1.2	1.1	1.1	1.14	1.32	1.18	1.2	1.34	1.26	1.28
D_{Meso} (nm)	33.7	6.4	–	>40	–	17	17	14	–	17	17	17	17

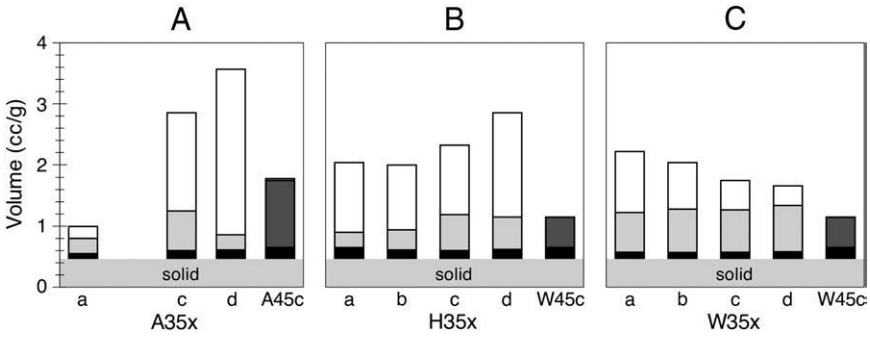

Fig. 3. Pore volume based on the micropores (black), mesopores (gray), and macropores (white and black). In A, the t-BuOH sample's macropore volume increases with the catalyst. This behavior is unusual in metal catalysis and is common of low catalyst concentration. Adding 8 mM of water, B, reduced the macropore volume while increasing the mesopore porosity. Lastly, the addition of water, C, at various levels from 2 to 11 mM further reduced the macropore volume increasing the mesopore porosity. The increase of solid content, dark gray, further reduced the appearance of macropores.

Structurally, there are marked differences between how the t-BuOH and water mixture alter HMTA and affect the porosity distribution within the gels. For example the increase in macropore volume under high concentration of catalyst in the organic solvent system suggests that the colloidal network produces large pores as those seen in low concentration catalysis in metal ion systems. Intuitively, it would be thought that a reduction in basicity is responsible for such increase. But as mentioned in The sol–gel process section the reaction times are not different enough to produce such radical change in the porosity. Another explanation besides pH and reaction rate are needed, TEM images can provide insights to how this macroporosity is developed.

3.3. Nanostructure shape

While the pore size and volume were estimated based on the nitrogen sorption the shape of the nanostructure also provide clues to the processes involved. TEM images of the pyrolyzed cryogels differed in structure to their metal ion catalyzed counterparts. First, large macropore volumes observed in the previous section required low concentration catalysis (RC = 200) as seen in Fig. 4A. In the HMTA catalyzed case $W_{35}d$ and $A_{35}d$, Fig. 4B and C, the colloidal particles were large but deformed. This deformation was observed at the high catalyst concentration of RH = 25. However the BET data suggested that these large colloids had much higher microporosity than the RF sample and that the micropore size decreased with increased catalyst amount. I.e. these are porous colloids or aggregates. In Fig. 4B the addition of water reduced the colloid size (consistent with the size reduction from the BET measurements) with an appearance that is similar to the RF gels. A sketch of the structural change is provided in Fig. 4.

The formation of aggregates under high catalysis might be an indication of a ligand type of catalyst or a reactive catalyst common in amine base catalysis and HMTA [12,15]. This is possible in the samples prepared in t-BuOH where HMTA is in a water deficient environment and carbon–nitrogen molecules can be produced. In the case where water is added to the system decomposition into ammonia is promoted and the system behaves more like a base catalyzed one as seen in the TEM images.

3.4. Bond differences and composition

The structural differences produced using various levels of catalyst and the addition of water are evident. But the chemical mechanisms involved in the polymerization are not clear. FTIR measurements showed the modifications of the chemical bonds of the dried organic cryogels catalyzed using HMTA. Two samples synthesized without hexamine are used to provide spectra of the polymer without the

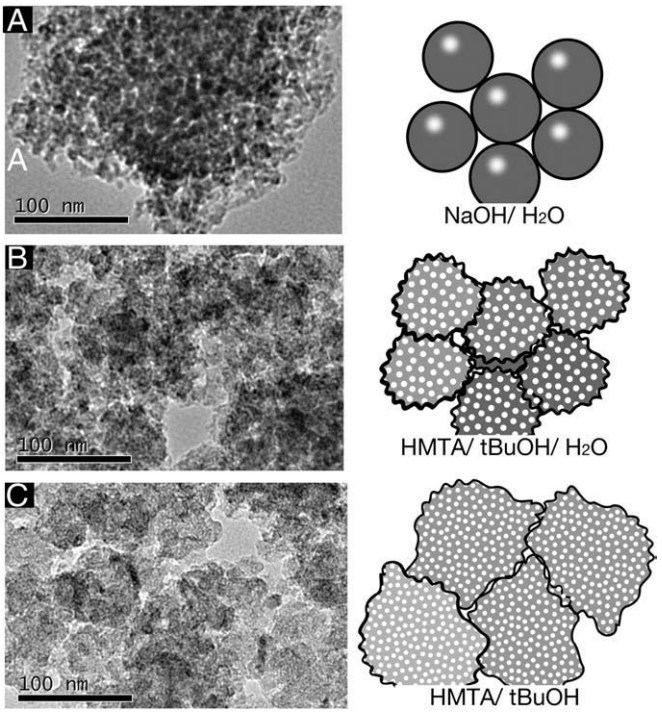

Fig. 4. TEM images of pyrolyzed RF carbon cryogel, A, and furaldehyde counterparts in water, B, and control, C, mixtures. Right, schematic representation of the particles produced by different syntheses. The deformation is similar to that observed by Wu et al. [5]. High concentrations of HMTA promote a larger more deformed structure.

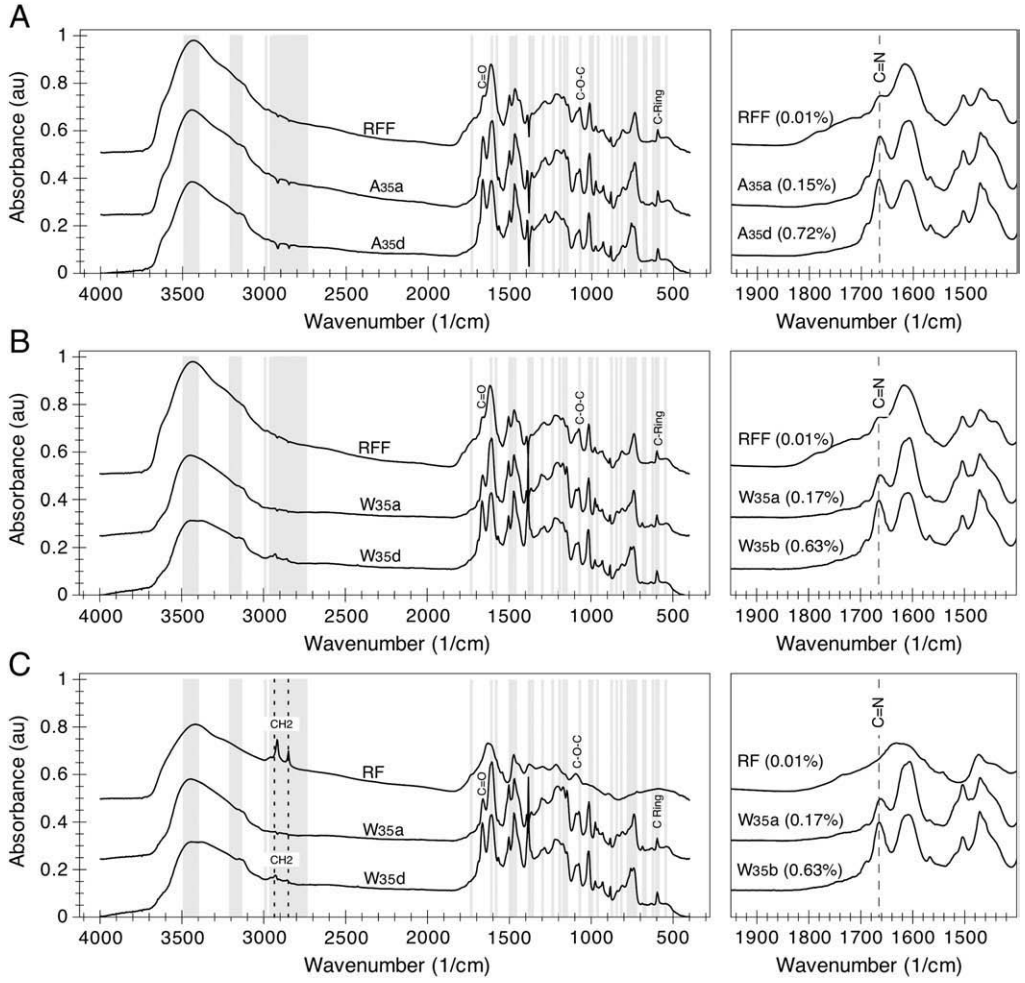

Fig. 5. Left, FTIR spectra of samples prepared in t-BuOH, A, t-BuOH and water B, and t-BuOH and water compared to RF, C. Right, peak at 1665 1/cm with CHN's% nitrogen in parenthesis.

hexamine effect. The samples are of resorcinol formaldehyde, RF, and resorcinol furaldehyde, RFF, two systems mainly composed of carbon rings and methylene bridges.

The effect of the organic solvent in the catalysis, Fig. 5A shows a comparison of the samples RFF using NaOH and those with hexamine. The FTIR spectra of the precursor molecules were compared to that of the resulting gels. In this correlation the ones using HMTA shared positions with those of the pure hexamine, furan and resorcinol rings. The peaks are listed in Table 4 (grayed areas in Fig. 5 [22,23]). Although most of the RFF's FTIR spectrum was correlated, there were three outstanding peaks. The peaks correspond to the wavenumbers 1665, 1078, and 598 1/cm. The two lowest wavenumbers are commonly assigned to C–O–C carbon chains and phenol rings respectively [4]. In addition both these bond were found in all three samples with and without hexamine in Fig. 5A. However, the peak at 1665 1/cm increased with the addition of hexamine and has been attributed to carbonyl groups C O [4]. In the case of the samples catalyzed using NaOH, RFF, this bond is expected and a small peak was found in the RFF spectra. However, the increase of the signal has also been attributed to a C N bond from an imino, a case possible since these bond types share the same wavenumber. Notice the 1665 1/cm peak's increase matches the N concentration of the dried organic cryogels using a CHN analyzer, Fig. 5. Although the nitrogen can be attributed to ammonia, notice the samples have been freeze dried under vacuum for seven day. Moreover, the chemical conditions in which the samples A_{35}ca and *d* with only the organic solvent were known to promote this decomposition of the hexamine [17,18]. Furthermore, in Fig. 5C the peaks resulting from CH_2 stretching (2924 and 2850 1/cm) of aliphatic compounds in the RF sample are missing in $A_{35}a$ and *d* the same in Fig. 5A. On the other hand, the peak produced at 1665 1/cm is not visible in the RF sample produced only with formaldehyde and resorcinol, same in Fig. 5C.

Table 4
Wavenumbers of dominant peaks for RF and RFF precursors.

Molecule	Formula	Wavenumber (1/cm)
Resorcinol	$C_6H_4(OH)_2$	3204, 1610, 1492, 1379, 1297, 1168, 1150, 961, 844, 776, 742, 681, 545
Furan	C_4H_4O	3140, 1580, 1480, 1375, 1192, 1070, 995, 875, 763, 747, 728, 623, 603, 590
Hexamine	$C_6H_{12}N_4$	2958, 2882, 1462, 1358, 1234, 1010, 816, 669
Formaldehyde	CH_2O	2990, 2850, 2783, 1732, 1496, 1235

The effect of water, $W_{35}a$ and *d*, in Fig. 5B and C, showed that the spectra had the same characteristics of the RFF gels but new features are formed that are in the resorcinol formaldehyde system. The aliphatic CH_2 stretch is now more visible perhaps indicating methylene like bridges like those in the RF system [23]. On the other hand the signal at the 1665 1/cm peak is less visible and the N concentration is lower in the high catalyst concentration sample $W_{35}d$. This can be an indication of decomposition of the hexamine into ammonia and formaldehyde in the water rich environment.

Although the FTIR data can't confirm the bond specie of the gels catalyzed using HMTA in t-BuOH, it does demonstrate that the spectrum changes from the ion base to the HMTA catalyzed and if water is added. The increase of the peak and concentration of nitrogen

does suggest that an imino anion or other nitrogen compound with a similar signal to C O or a C N might be present. This can also explain the change in color of the gels from yellow-orange to brown during the synthesis and the fact that large colloids are formed under high catalysis when pure t-BuOH is used. When using the t-BuOH the catalyst can retain its chemical structure or decompose into a heterocyclic structure. The later can be responsible for the formation of aggregates via a reactive catalyst [12,15], while in water the decomposition from HMTA to ammonia and formaldehyde promotes a catalysis similar to that of a base.

4. Conclusion

In this study it has been demonstrated that hexamethylenetetramine can have multiple catalytic effects in the polycondensation of resorcinol furaldehyde to produce carbon cryogels. The resulting carbons have tunable structure that exceeds that observed in the literature thanks to such decomposition reactions of HMTA when two solvent chemistries are used.

The first corresponds to that in pure tert-butanol in which a reactive catalyst produce a nanostructure that combines fine micropores <2 nm with the added benefit of high macropore volumes (with porosities exceeding 70%) that reduce the syneresis and subsequent shrinkage of the gels during drying. A feature uncommon in metal ion catalyzed gels. In addition the color change in the gel and FTIR spectra suggest new molecules or bonds from those found in the metal ion catalyzed gels using same precursor monomers. The yellow-orange color and peak at the 1665 1/cm peak suggest an imine or imino a possible product of hexamine's protonation.

Second, during the addition of water, the hexamine is allowed to decompose into formaldehyde and ammonia, the pore structure resembles a based catalyzed system and the macropore volume is significantly reduced with ca 20% porosity. Moreover, the later also reduces the mesopore size to less than 7 nm a desirable trait in applications such as energy storage where the pore size can limit the performance of the device. The chemical analysis also shows changes that another chemical species is produced. The coloration is more subdue and the absorbance peak in the 1665 is reduced in magnitude.

These combined characteristics of HMTA catalysis can produce a wider range of pore sizes and volumes, while retaining high surface areas.

Acknowledgments

This work has been supported in part by the University of Washington Bioenergy IGERT (DGE-0654252). This work was supported financially in part by the Department of Energy (DE-FG02-07ER46467), National Science Foundation (DMI-0455994 and DMR-0605159), Air Force Office of Scientific Research (AFOSR-MURI, FA9550-06-1-0326), Pacific Northwest National Laboratories (PNNL), National Center for Nanomaterials Technology (NCNT, Korea), Washington Research Foundation (WRF), the University of Washington (TGIF), IntelCorporation, EnerG2, Dr. Zimin Nie from PNNL (BET analysis), Chen Fang (FTIR UW MSE, Miqin Zhang's group), Jim Hull (XPS measurements, NESAC/BIO grant number EB-002027) and Dongsen Xu (CHN, School of Forest Resources College of Environment).

Appendix A. Additional structural data

Table 5
Structural data of pyrolyzed samples with solid concentrations of 35 and 45%.

	ρ (cm^3/g)	S_{BET} (m^2/g)	V_{Micro} (cm^3/g)	V_{Meso} (cm^3/g)	P_{Micro} (%)	P_{Meso} (%)	P_{Macro} (%)	D_{Micro} (nm)	D_{Meso} (nm)
RF	0.07	567	0.06	1.17	0	8	88	1.46	9.39
RFF	0.75	528	0.23	0.36	17	27	22	1.5	–
$C_{45}c$	0.56	575	0.2	1.1	11	59	5	1.20	33.7
$W_{45}c$	0.87	583	0.2	0.5	17	43	0	1.20	6.4
$C_{35}a$	1.0	380	0.10	0.25	10	25	20	1.58	–
$C_{35}c$	0.35	593	0.21	1.6	5	23	56	1.2	>40
$C_{35}d$	0.28	633	0.32	0.21	4	7	76	1.1	–
$H_{35}a$	0.49	521	0.2	0.25	10	12	56	1.10	17.0
$H_{35}b$	0.50	470	0.16	0.33	8	17	56	1.14	17.0
$H_{35}c$	0.38	598	0.15	0.59	6	25	49	1.32	14.0
$H_{35}d$	0.35	601	0.17	0.53	6	19	60	1.18	–
$W_{35}a$	0.45	575	0.14	0.74	6	29	45	1.20	17.0
$W_{35}b$	0.49	542	0.12	0.71	6	35	37	1.34	17.0
$W_{35}c$	0.57	593	0.14	0.8	7	40	27	1.26	17.0
$W_{35}d$	0.69	532	0.13	0.76	8	46	19	1.28	17.0

ρ = bulk density, S_x = surface area, P_x = porosity, and D_x = pore diameter.

References

[1] A.F. Burke, Proc IEEE 95 (2007) 806.
[2] B.B. Garcia, A.M. Feaver, R.D. Champion, Q. Zhang, T.T. Fister, K.P. Nagle, G.T. Seidler, G. Cao, J. Appl, Phys. 104 (2008) 014305.
[3] B.E. Conway, Electrochemical Supercapacitors Scientific Fundamentals and Technological Applications, Plenum Press, 1999.
[4] H.Y. Tian, C.E. Buckley, S. Mule, M. Paskevicius, B.B. Dhal, Nanotechnology 19 (2008) 475605.
[5] D. Wu, R. Fu, S. Zhang, M. Dresselhaus, G. Dresselhaus, J. Non-Cryst. Solids 336 (2004) 26.
[6] N. Job, A. Thery, R. Pirard, J. Marien, L. Kocon, J. Rouzaud, F. Beguin, J. Pirard, Carbon 43 (2005) 2481.
[7] C.J. Brinker, G.W. Scherer, Sol–Gel Science: the Physics and Chemistry of Sol–Gel Processing, Academic Press, 1990.
[8] J.K. Fink, Reactive Polymers Fundamentals and Applications — a Concise Guide to Industrial Polymers, William Andrew Publishing/Plastics Design Library, 2005.
[9] M.A. Czarnecki, D. Wojtkow, J. Mol. Struct. 883 (2008) 203.
[10] L. Wojnarovits, E. Takacs, K. Dajka, S. Emmi, M. Russo, M. D'Angelantonio, Radiat. Phys. Chem. 69 (2004) 217.
[11] D. Wojtkow, M.A. Czarnecki, J. Phys. Chem. A 110 (2006) 10552.
[12] N. Blažzević, D. Kolbah, B. Belin, V. Šunjić, F. Kajfež, Synthesis 1979 (1979) 161.
[13] P. Haas, W. Pitt, S. Robinson, A. Ryon, Ind. Eng. Chem. Res. 22 (1983) 461.
[14] F. Ullmann, W. Gerhartz, Y.S. Yamamoto, F.T. Campbell, R. Pfefferkorn, J.F. Rounsaville, Ullmann's Encyclopedia of Industrial Chemistry, VCH, 2007.
[15] S.E. Denmark, G.L. Beutner, Angew. Chem-Int. Edit. 47 (2008) 1560.
[16] F.A. Carey, R.J. Sundberg, Advanced Organic Chemistry — Part B: Reactions and Synthesis, Springer-Verlag, 2007.
[17] X. Zhang, M. Looney, D. Solomon, A. Whittaker, Polymer 38 (1997) 5835.
[18] X. Zhang, D. Solomon, Chem. Mat. 11 (1999) 384.
[19] G.Q. Lu, X.S. Zhao, Nanoporous Materials Science and Engineering, Imperial College Press, 2004.
[20] M. Grigoras, N. Antonoaia, Eur. Polym. J 41 (2005) 1079.
[21] S.A. Al-Muhtaseb, J.A. Ritter, Adv. Mater. 15 (2003) 101.
[22] Properties of Organic Compounds on CD-ROM, Chapman & Hall/CRC, 2001.
[23] J. Coates, Interpretation of Infrared Spectra, a Practical Approach in Encyclopedia of Analytical Chemistry, John Wiley & Sons Ltd, 2000.